Proc. IUTAM Symposium on non-steady flow of water at high speeds Leningrad, USSR. 1971

WALL EFFECTS IN CAVITY FLOWS AND THEIR CORRECTION RULES

T. YAO-TSU WU, A. K. WHITNEY AND C. BRENNEN
California Institute of Technology, Pasadena, Cal., USA

1. Introduction

The wall effects in cavity flows have been long recognized to be more important and more difficult to determine than those in single-phase, non-separated flows. Earlier theoretical investigations of this problem have been limited largely to simple body forms in plane flows, based on some commonly used cavity-flow models, such as the Riabouchinsky, the reentrant jet, or the linearized flow model, to represent a finite cavity. Although not meant to be exhaustive, references may be made to Cisotti (1922), Birkhoff, Plesset and Simmons (1950, 1952), Gurevich (1953), Cohen et al. (1957, 1958), and Fabula (1964). The wall effects in axisymmetric flows with a finite cavity has been evaluated numerically by Brennen (1969) for a disk and a sphere. Some intricate features of the wall effects have been noted in experimental studies by Morgan (1966) and Dobay (1967). Also, an empirical method for correcting the wall effect has been proposed by Meijer (1967).

The presence of lateral flow boundaries in a closed water tunnel introduces the following physical effects: (i) First, in dealing with the part of irrotational flow outside the viscous region, these flow boundaries will impose a condition on the flow direction at the rigid tunnel walls. This "streamline-blocking" effect will produce extraneous forces and modifications of cavity shape. (ii) The boundary layer built up at the tunnel walls may effectively reduce the tunnel cross-sectional area, and generate a longitudinal pressure gradient in the working section, giving rise to an additional drag force known as the "horizontal buoyancy". (iii) The lateral constraint of tunnel walls results in a higher velocity outside the boundary layer, and hence a greater skin friction at the wetted body surface. (iv) The lateral constraint also affects the spreading of the viscous wake behind the cavity, an effect known as the "wake-blocking". (v) It may modify the location of the "smooth detachment" of cavity boundary from a continuously curved body.

In the present paper, the aforementioned effect (i) will be investigated for the pure-drag flows so that this primary effect can be clarified first. Two cavity flow models, namely, the Riabouchinsky and the open-wake (the latter has been attributed, independently, to Joukowsky, Roshko, and Eppler) models, are adopted for detailed examination. The asymptotic representations of these theoretical solutions, with the wall effect treated as a small correction to the unbounded-flow limit, have yielded two different wall-correction rules, both of which can be applied very effectively in practice. It is of interest to note that the most critical range for comparison of these results lies in the case when the cavitating body is slender, rather than blunt ones, and when the cavity is short, instead of very long ones in the nearly choked-flow state. Only in this critical range do these flow models deviate significantly from each other, thereby permitting a refined differentiation and a critical examination of the accuracy of these flow models in representing physical flows. A series of experiments carefully planned for this purpose has provided conclusive evidences, which seem to be beyond possible experimental uncertainties, that the Riabouchinsky model gives a very satisfactory agreement with the experimental

results, and is superior to other models, even in the most critical range when the wall effects are especially significant and the differences between these theoretical flow models become noticeably large.

These outstanding features are effectively demonstrated by the relatively simple case of a symmetric wedge held in a non-lifting flow within a closed tunnel, which we discuss in the sequel.

2. Riabouchinsky Model

The two-dimensional symmetric cavity flow in question is depicted in fig. 1 for the physical plane $z = x + iy$, the complex potential plane $f = \phi + i\psi$, and a related parametric complex plane $\zeta = \xi + i\eta$. For a cavitat-

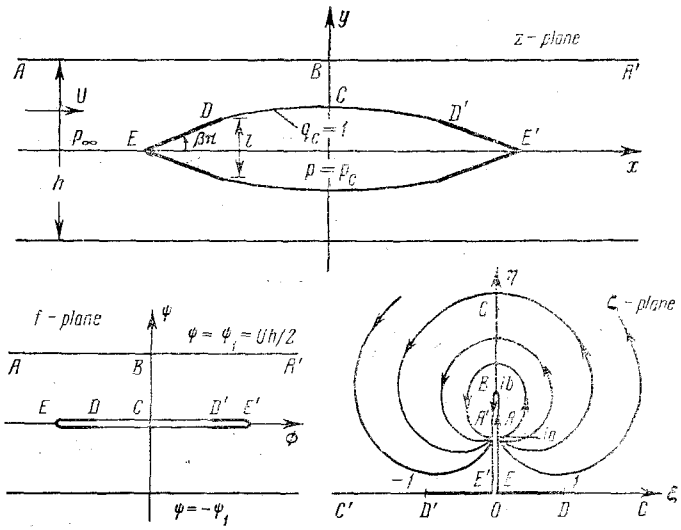

Fig. 1. The Riabouchinsky model for pure-drag cavity flow in a tunnel.

ing wedge of halfvertex angle $\beta\pi$, base chord l, placed symmetrically in a flow bounded within a tunnel of spacing h, the parametric solution is readily found as

$$\frac{df}{d\zeta} = A\zeta(\zeta^2+a^2)^{-1}(\zeta^2+b^2)^{-1/2}, \quad A = \frac{1}{\pi}Uh(b^2-a^2)^{1/2}, \tag{1}$$

$$w(\zeta) = \frac{df}{dz} = e^{-i\beta\pi}\{\zeta/[1+(1-\zeta^2)^{1/2}]\}^{2\beta} \qquad (0<\beta<1), \tag{2}$$

where the real, positive constants a, b are related to the upstream velocity U and the maximum velocity V along the wall at point B by

$$U = U(a) = \{a/[1+(1+a^2)^{1/2}]\}^{2\beta}, \text{ or } a = a(U) = 2(U^{-1/2\beta}-U^{1/2\beta})^{-1}, \tag{3}$$

$$V = U(b) \quad \text{or} \quad b = a(V). \tag{4}$$

The base-chord to tunnel-spacing ratio can be determined from (1), (2) to yield

$$\lambda \equiv \frac{l}{h} = \frac{2U}{\pi}(\sin\beta\pi)(b^2-a^2)^{1/2} I_+(a, b), \tag{5}$$

where I_+ (and I_- for other flow quantities) is given by

$$I_\pm(a, b) = \int_0^1 \frac{[1\pm(1-\zeta^2)^{1/2}]^{2\beta}\,\zeta^{1-2\beta}}{(\zeta^2+a^2)(\zeta^2+b^2)^{1/2}}\,d\zeta. \tag{6}$$

The drag coefficient, $C_D = D\Big/\left(\frac{1}{2}\,\rho U^2 l\right)$, is obtained by direct integration of the pressure as

$$C_D(\sigma, \lambda) = (1 + \sigma)\,[1 - I_-(a, b)/I_+(a, b)], \tag{7}$$

where the cavitation number σ is defined, as usual, by

$$\sigma \equiv (p_\infty - p_c)\Big/\left(\frac{1}{2}\,\rho U^2\right) = U^{-2} - 1 \equiv \sigma(U), \tag{8}$$

p_∞ being the free stream pressure, p_c the constant cavity pressure, with the corresponding velocity q_c on the cavity boundary. Henceforth, q_c will be normalized to unity for simplicity.

The choked flow state (i.e. when the cavity becomes infinitely long in a closed tunnel) is reached as $V \to 1$, or $b \to \infty$. The expression (5) for λ in the limit as $b \to \infty$ is obviously

$$\lambda = U_* F(U_*), \tag{9}$$

where

$$F(U) = F(U(a)) \equiv \tag{10}$$

$$\equiv \frac{2}{\pi}\sin\beta\pi \int_0^1 [1 + (1-\zeta^2)^{1/2}]^{2\beta}\,\frac{\zeta^{1-2\beta}}{\zeta^2 + a^2}\,d\zeta.$$

The quantity U_*, and hence $a_* = a(U_*)$ by (3), denotes the choked-flow limit of U as determined by (9), (10) and (3) to give $U_* = U_*(\beta, \lambda)$ as a function of β and λ. The corresponding limit of cavitation number, $\sigma_* = \sigma(U_*)$ by (8), is called the "choking cavitation number" (or the "blockage constant"), which is also a function of β and λ, say $\sigma_* = \sigma_*(\beta, \lambda)$. The corresponding drag coefficient at the choked-flow state can be derived directly by a momentum consideration to yield

$$C_{D_*}(\beta, \lambda) = \frac{1}{\lambda}\left(\frac{1}{U_*} - 1\right)^2, \tag{11}$$

which is of course also the choked-flow limit of (7) as $b \to \infty$. The choked-flow results (9)-(11) are shown in fig. 2. Both $\sigma_*(\beta, \lambda)$ and $C_{D_*}(\beta, \lambda)$ increase as β increases (with λ fixed), or as λ increases (with β fixed). When both β and λ are kept fixed, the cavity flow is finite in length for $\sigma > \sigma_*$, infinite at $\sigma = \sigma_*$, and no cavity flow is physically feasible for $\sigma < \sigma_*$. It is further noted that the above choked-flow solution is common to all theoretical flow models in the same limit.

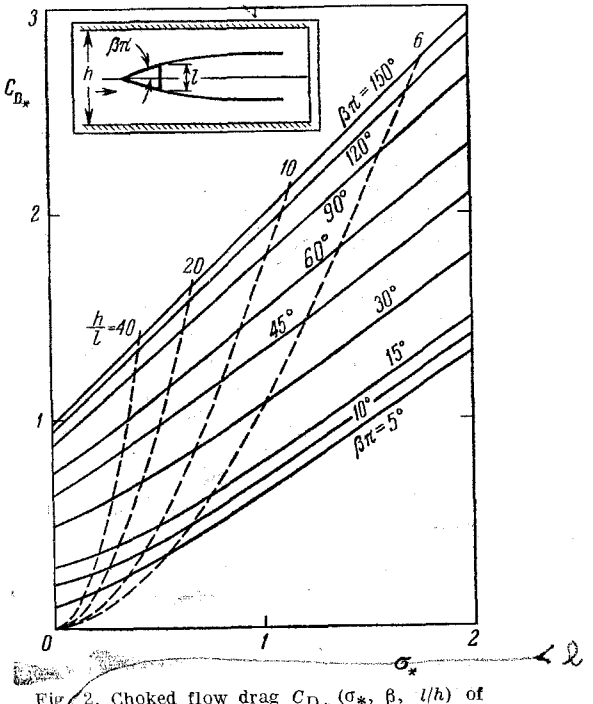

Fig. 2. Choked flow drag $C_{D_*}(\sigma_*, \beta, l/h)$ of wedges versus the choked cavitation number $\sigma_*(\beta, l/h)$. Cavity is finite in length for $\sigma > \sigma_*$.

On the other hand, the unbounded-flow limit $\lambda = 0$ is reached as $b \to a$, which implies $V \to U$, or $\sigma'' \to \sigma$, where σ'', defined by

$$\sigma'' \equiv (p_b - p_c)\Big/\left(\frac{1}{2}\,\rho V^2\right) = V^{-2} - 1 = \sigma(V), \tag{12}$$

is a new cavitation number based on the minimum pressure p_b and maximum velocity V along the tunnel wall at point B of fig. 1. For small λ, an asymptotic representation of the drag coefficient can be derived from the above exact

solution by first expanding $C_D(\sigma, \lambda)/(1+\sigma)$ in Taylor's series,

$$(13)\qquad \frac{C_D(\sigma,\lambda)}{1+\sigma}=\frac{C_D(\sigma,0)}{1+\sigma}+(\sigma''-\sigma)\left[\frac{\partial}{\partial\sigma''}\left(\frac{C_D(\sigma,\lambda)}{1+\sigma}\right)\right]_{b=a}+O[(\sigma''-\sigma)^2].$$

From (7) and (6) it follows that

$$(14)\qquad \left[\frac{\partial}{\partial\sigma''}\frac{C_D(\sigma,\lambda)}{1+\sigma}\right]_{b=a}=-\left[\frac{\partial}{\partial b}\left(\frac{I_-(a,b)}{I_+(a,b)}\right]\frac{db}{d\sigma''}\right]_{b=a}=$$

$$=-\left[\frac{1}{3}\frac{(a)}{da}\frac{I_-(a,a)}{I_+(a,a)}\right]\frac{da}{d\sigma}=\frac{1}{3}\frac{d}{d\sigma}\frac{C_D(\sigma,0)}{1+\sigma}.$$

Upon substituting (14) in (13), the resulting expression on the right hand side of (13) can be regarded as an expansion of $C_D(\sigma', 0)/(1+\sigma')$ for small $|\sigma'-\sigma|$, and hence

$$(15)\qquad \frac{C_D(\sigma,\lambda)}{1+\sigma}=\frac{C_D(\sigma',0)}{1+\sigma'}+O(\lambda^2),$$

where

$$(16)\qquad \sigma'=\sigma+\frac{1}{3}(\sigma''-\sigma)=\frac{2}{3}\sigma+\frac{1}{3}\sigma''.$$

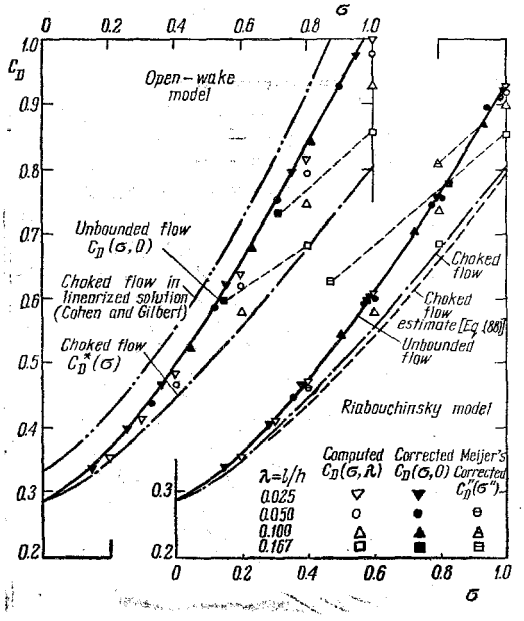

Fig. 3. Correction rules tested against theoretical results for 30° wedge.

Equations (15), (16) are the desired wall-correction rule, which takes a measured drag coefficient $C_D(\sigma, \lambda)$, in a tunnel of known λ, and converts it by (15) to an estimated unbounded drag coefficient $C_D(\sigma', 0)$ of the same wedge in unbounded flow ($\lambda = 0$) at a different cavitation number, σ', given by (16) as a linear combination of the cavitation number σ in bounded flow and σ''. The new cavitation number σ'' can be acquired either by actual measurement together with σ in experiments or by calculation from (4) and (5).

An example of use of this rule in estimating the unbounded drag coefficient from the exact values of $C_D(\sigma, \lambda)$ calculated from (7) and (5) is shown in fig. 3 for $\beta\pi = 15°$. The agreement of predicted $C_D(\sigma', 0)$ by (15), (16) with the calculated exact values of $C_D(\sigma, \lambda)$ from (7) and (5) is found to be excellent for all angles, with λ up to 1/6 and σ up to 1. Also shown in fig. 3 is the empirical rule of Meijer (1967), which is based on a different drag coefficient $C_D''(\sigma'')$ as a function of the cavitation number σ'' according to

$$(17)\qquad C_D''(\sigma'')=D\Big/\left(\tfrac{1}{2}\rho V^2 l\right),\quad \sigma''=(p_b-p_c)\Big/\left(\tfrac{1}{2}\rho V^2\right),$$

where D is the drag measured at cavitation number σ, p_b is the minimum pressure and V is the corresponding maximum velocity on the tunnel wall (this σ'' agrees with the definition (12) for the theoretical Riabouchinsky model). As shown in fig. 3, Meijer's rule is found to over-correct the wall effect predicted by the Riabouchinsky model, while the latter is well supported by the experimental results, as will be discussed more fully later.

3. Open-Wake Model

The same physical flow as dealt with in the previous case is shown in fig. 4 for the open-wake model, with the parametric ζ-plane denoted by the same symbol, except it is now referred to the present flow model. The parametric solution in this case is found to be

$$\frac{df}{d\zeta} = A\zeta(\zeta^2+a^2)^{-1}(\zeta^2+b^2)^{-1}, \quad A = \frac{1}{\pi}Uh(b^2-a^2), \tag{18}$$

and the complex velocity $w = w(\zeta)$ for the cavity flow past a wedge is again given by (2). It thus follows that the functional forms of $U(a)$ and $V = U(b)$

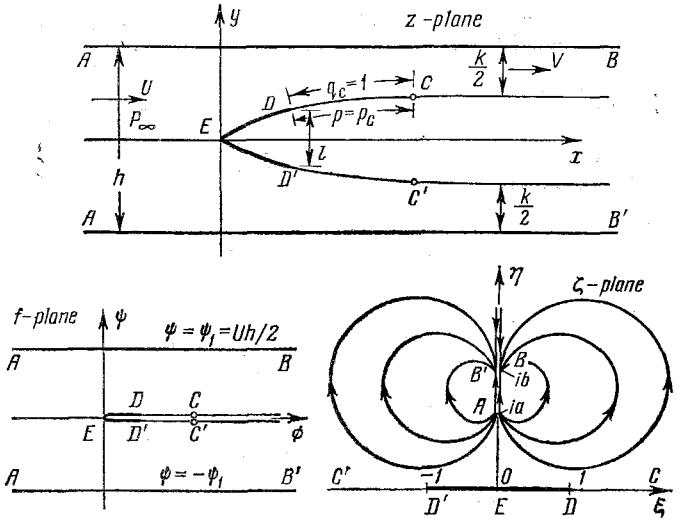

Fig. 4. The open-wake model for pure drag flows in a tunnel.

are the same as (3), (4) given before. The velocity V also gives the maximum value on the wall, but now at downstream infinity. The base-chord-to-tunnel-spacing ratio is found to be

$$\lambda = l/h = U[F(U) - F(V)], \tag{19}$$

where $F(U)$ is given by (10). The drag coefficient can be obtained directly by the momentum consideration as

$$C_D(\sigma, \lambda) = \frac{1}{\lambda}\left(\frac{V}{U}-1\right)\left(\frac{1}{UV}-1\right). \tag{20}$$

Upon eliminating V between (19), (20), the result provides $C_D(\sigma, \lambda)$ with the wall effect.

The choked-flow state of this model is reached also as $b \to \infty$, or equivalently, as $V \to 1$. The corresponding limit of a and U, denoted by a_* and U_* respectively, are readily seen to be given again by (9), (10), while the drag coefficient of (20) reduces to (11). The choked-flow state of these two models, in fact of all theoretical models, are the same.

When λ $(=l/h)$ is small, as is usually the case in experimental practice, the asymptotic representation of the preceding exact solution can be derived as follows. First, by substituting (19) for λ in (20), the unbounded-flow limit (as $\lambda \to 0$, or equivalently, as $V \to U$) of the drag coefficient $C_D(\sigma, \lambda)$ of

wedges is obtained by letting $V \to U$, giving, upon using l'Hospital's rule,

$$C_D(\sigma, 0) = -U^{-2}(U^{-2}-1)\left[\frac{dF(U)}{dU}\right]^{-1}.$$

If this equation is solved for $F'(U)$, and integrated from U to V, an alternative expression for λ is obtained (using again (19)),

$$\lambda = U\int_U^V \frac{u^{-2}(u^{-2}-1)}{C_D(\sigma(u), 0)}\,du, \tag{21}$$

where $\sigma(u) = u^{-2} - 1$. For given wedge angle, (21) determines V implicitly as a function of σ and λ. Next, partial differentiation of (20) and (21) with respect to σ and λ and elimination of terms involving V gives a parital differential equation for $C_D(\sigma, \lambda)$, which reduces in the limit as $\lambda \to 0$ to

$$\frac{\partial}{\partial\lambda}C_D(\sigma, 0) + \frac{1+\sigma}{\sigma}C_D(\sigma, 0)\frac{\partial}{\partial\sigma}C_D(\sigma, 0) = \frac{1}{\sigma}C_D^2(\sigma, 0). \tag{22}$$

Now, by integrating (22) from σ' to σ ($>\sigma'$, with $\sigma - \sigma' = O(\lambda)$) along the mathematical characteristics of (22):

$$\frac{d\sigma}{d\lambda} = \frac{1+\sigma}{\sigma}C_D(\sigma, 0), \quad \frac{dC_D}{d\sigma} = \frac{C_D(\sigma, 0)}{1+\sigma},$$

we obtain

$$C_D(\sigma', 0) = \frac{1+\sigma'}{1+\sigma}C_D(\sigma, \lambda) + O(\lambda^2), \tag{23}$$

where

$$\sigma' = \sigma - \left(\frac{1+\sigma'}{\sigma'}\right)C_D(\sigma', 0)\,\lambda + O(\lambda^2), \tag{24a}$$

or, to the same order of accuracy,

$$\sigma' = \sigma - \left(\frac{1+\sigma}{\sigma}\right)C_D(\sigma, \lambda)\,\lambda + O(\lambda^2). \tag{24b}$$

Thus, (23) and (24) play the same role of a two-way correction from $C_D(\sigma, \lambda)$ in a bounded flow to $C_D(\sigma', 0)$ in unbounded flow, and vice versa, as in the case of (15), (16) based on the Riabouchinsky model. In fact, (15) and (23) are identical up to the order $O(\lambda)$. An essential difference between these two sets of rules, in the sense of their prerequisite for application, arises from the significance of σ' in these two cases. For the Riabouchinsky model, it is necessary to make an additional measurement of a new cavitation number σ'', whereas in the case of the open-wake model, no such additional measurement is required.

The wall corrections predicted by (23) and (24) have been computed for the same configuration of $\beta\pi = 15°$; the result, as shown in fig. 3, is again in excellent agreement with the exact solution, (19) and (20), for λ up to 1/6 and σ up to 1. In fact, the accuracy of the rule (23), (24) is uniformly good for all wedge angles. More specifically, the following features of the wall effects predicted by these two theoretical flow models are of interest to note.

4. Main Features of the Theoretical Results of Wall Effects

While the over-all accuracy of the two sets of wall correction rules (namely, (15), (16) for the Riabouchinsky model and (23), (24) for the openwake model) has been established by comparison with their respective exact solution, direct comparison of the drag coefficients based on these cavity flow models, however, exhibits refined differences. A detailed comparison between the Riabouchinsky

and open-wake models is given for the representative cases of 30° and 90° wedges, as shown in fig. 5.

As can be seen from this comparison, the open-wake model predicts, in general, greater drag coefficients than the Riabouchinsky model, other quantities being equal. This difference is actually inherent to their predictions of the unbounded flow. More specifically, starting from the same limit of the choked-flow state, the difference between these two flow models becomes more appreciable for thinner wedges (smaller β) and shorter cavities (larger σ), reaching the widest discrepancy as $\lambda \to 0$ when the unbounded-flow limit is approached.

This inherent difference notwithstanding, the results of these two flow models exhibit the following similar features of the wall effect. First, the effect of the lateral constraint by the tunnel walls is to make C_D lower than in an unbounded flow at the same cavitation number. Actually, this streamline blocking effect results in an increase of flow velocity, and hence a decrease of pressure over the wetted surface of body, and also causes the cavity pressure to be somewhat lower than in an unbounded flow with the same free stream condition. These two effects reinforce each other to yield a lower C_D at the same σ.

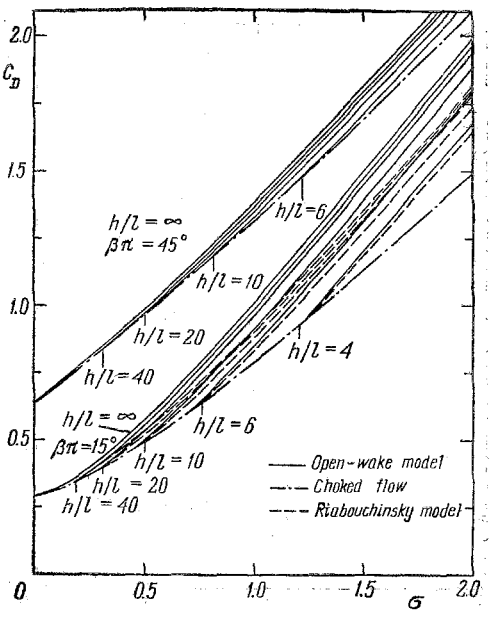

Fig. 5. Comparisons of the drag coefficient for 30° and 90° wedges based on the different models.

Another remarkable feature of the results is that the percentage drag reduction due to the wall effect, for fixed σ and λ, actually increases with decreasing wedge angle. Physically, this is likely due to two reasons: first, a thinner body has longer wetted surface exposed to the wall effect, and second, the singularity of the cavity-boundary curvature becomes weaker for thinner bodies at the point of detachment. The former feature is actually borne out by the experimental measurements of pressure distribution. In contrast, the wall effects become increasingly smaller as β increases for blunter wedges, and fall to insignificant magnitude for $\beta\pi > 90°$.

5. Experimental Verification; a Critical Examination of the Flow Models

In attempt to verify the theoretical results and to conduct a critical examination of the cavity flow models in regard to their accuracy in representing physical flow, a series of experiments was carried out with due consideration of the viscous effects, which generate a boundary layer on the body surface and along the tunnel wall, and other real-fluid effects. Four wedges of vertex angles $2\beta\pi = 7\frac{1}{2}°$, 9°, 15° and 30° (chord ~6 in.) were tested in the 6 in. span, two-dimensional working section of a high-speed water tunnel for a set of values of $\lambda = l/h$. The values of drag coefficient on these wedges were obtained both by pressure integration and by direct balance measurement, with the viscous drag estimated and subtracted in the latter method. The results by pressure integration were found to be more accurate, as indicated by its repeata-

bility, whereas the direct force measurements showed more scatter of data. Also, a series of static pressure taps on the lower wall of the tunnel were used for the purpose of determining the wall pressure distribution.

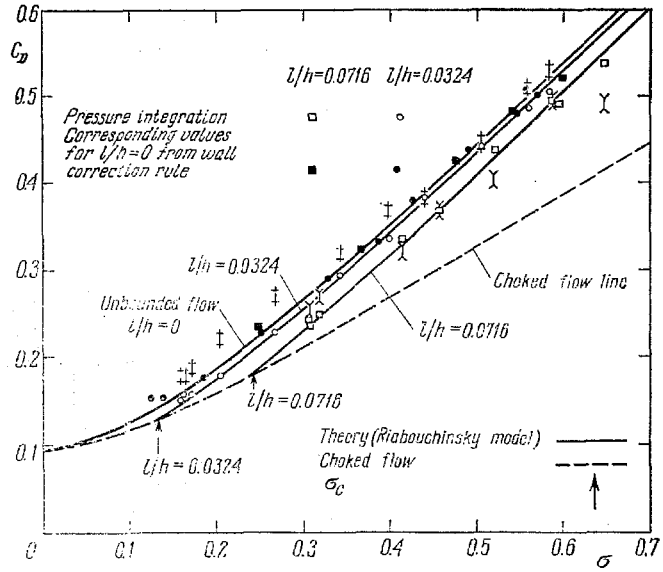

Fig. 6. Drag coefficient of the 9° wedge ($\beta\pi = 4.5°$).

As shown in figs 6, 7 for two representative cases of $2\beta\pi = 9°$ and 30° wedges, the Riabouchinsky model yields results closest to the experimental measurements over a range of λ up to values as high as $\lambda = 0.236$. For clarity,

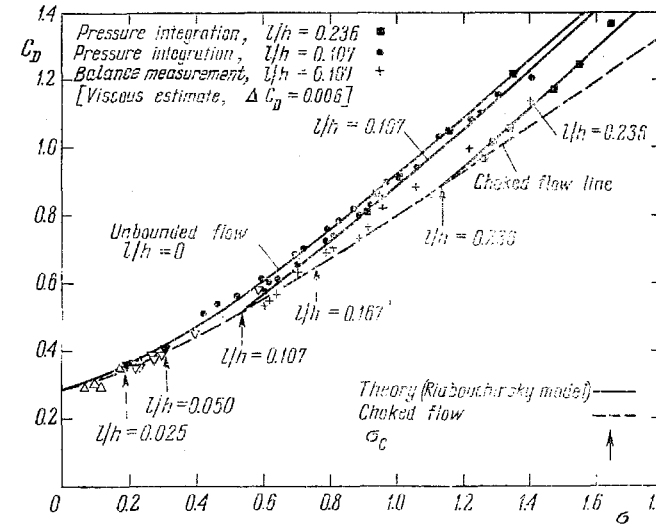

Fig. 7. Drag coefficient of the 30° wedge ($\beta\pi = 15°$).

comparison is made only with that model, as the extent of difference between the two models is already known. In addition, comparison is also made with the results of the linearized theory of Cohen and Gilbert (1957). As shown in fig. 3, the linearized theory yields values of C_D appreciably greater than either

the exact theory or the experiments. The difference is of course less for wedges of smaller vertex angle.

The pressure-integrated drag on the 9° and 30° wedges are corrected for wall effects using the relations (23), (24) and the experimental values of minimum wall pressure. The results are the solid points in fig. 6 and fig. 7. Clearly

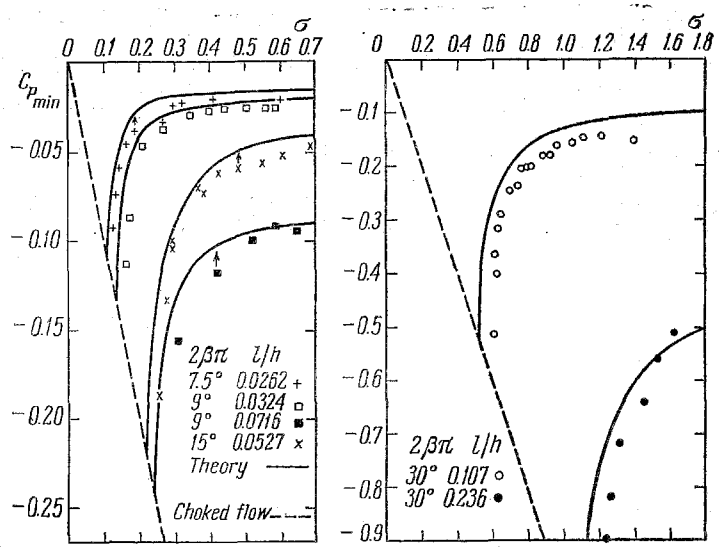

Fig. 8. Minimum wall pressure versus cavitation number. Arrows indicate corresponding curves.

the results are very satisfactory, since the rule collapses the points for different $\lambda = l/h$ onto a single line very close to the unbounded-flow theoretical line. We further note that the theoretically predicted values of minimum wall pressure are in good agreement with the experiments, as shown in fig. 8.

Although the experimental investigation has been limited to symmetric wedges only, the correction rule (23), (24) is expected to possess a wider validity, at least for symmetric bodies without too large curvatures, since the geometry of the body profile is only implicitly involved in the correction formula.

The early part of the main theoretical study was carried out under the support of the Naval Ship System Command General Hydrodynamics Research Program, administered by the Naval Ship Research and Development Center, and the latter part under the support of the Office of Naval Research. The experimental investigation using the High-Speed Water Tunnel facility of the Hydrodynamics Laboratory was supported by the Division of Engineering and Applied Science of the California Institute of Technology. To these sources of support and encouragement the authors have pleasure in expressing their appreciation and gratitude.

REFERENCES

1. G. Birkhoff, M. S. Plesset and N. Simmons. Wall Effects in Cavity Flows, I.— Quart. Appl. Math., 1950, 8, 161.
2. G. Birkhoff, M. S. Plesset and N. Simmons. Wall Effects in Cavity Flow, II.— Quart. Appl. Math., 1952, 9, 413.
3. C. Brennen, A Numerical Solution of Axisymmetric Cavity Flows.— J. Fluid Mech., 1969, 37, 115.
4. U. Cisotti. Idromeccanica Piana. Milan, 1922.
5. H. Cohen and R. Gilbert. Two-dimensional, Steady, Cavity Flow about Slender Bodies in Channels of Finite Breadth.— J. Appl. Mech., 1957, 24, 170.

6. H. Cohen, C. C. Sutherland and Y. Tu Wall Effects in Cavitating Hydrofoil Flow — J. Ship Res., 1957, 3, 31.
7. H. Cohen and R. C. DiPrima. Wall Effects in Cavitating Flows.— Proc. 2nd Symp. on Naval Hydrodynamics, ACR-38. Washington, D.C.: Govt. Printing Office, 1958.
8. G. V. Dobay. Experimental Investigation of Wall Effect on Simple Cavity Flows.— Proc. Symp. Testing Techn. in Ship Cavitation Research, 1, Skipsmodelltanken, Tronheim, Norway, 1967, p. 175.
9. A. G. Fabula. Choked Flow about Vented or Cavitating Hydrofoils.— Trans. ASME, Series D, 1964, 86, 561.
10. M. I. Gurevich.— Proc. A. I. Mikoyan, Moscow Tech. Inst. Fis. Ind. Econ., V, 1953. [М. И. Гуревич. Сопротивление цилиндра и клина при малых числах кавитации.— Труды Моск. технич. ин-та рыбной промышленности и хозяйства им. А. И. Микояна, вып. 5, 1953.]
11. M. C. Meijer.— Pressure Measurements on Flapped Hydrofoils in Cavity Flows and Wake Flows.— J. Ship Res., 1967, 11, 170.
12. W. B. Morgan. The Testing of Hydrofoils and Propellers for Fully-Cavitating or Ventilated Operation.— Proc. 11th ITTC, Tokyo, 1966, p. 202.